Biomaterials 93 (2016) 48–59

Contents lists available at ScienceDirect

Biomaterials

journal homepage: www.elsevier.com/locate/biomaterials

A FRET-guided, NIR-responsive bubble-generating liposomal system for *in vivo* targeted therapy with spatially and temporally precise controlled release

Er-Yuan Chuang [a, 1], Chia-Chen Lin [a, 1], Ko-Jie Chen [a, 1], De-Hui Wan [b], Kun-Ju Lin [c, d], Yi-Cheng Ho [e], Po-Yen Lin [a], Hsing-Wen Sung [a, b, *]

[a] Department of Chemical Engineering, National Tsing Hua University, Hsinchu, Taiwan, ROC
[b] Institute of Biomedical Engineering, National Tsing Hua University, Hsinchu, Taiwan, ROC
[c] Department of Medical Imaging and Radiological Sciences, College of Medicine, Chang Gung University, Taoyuan 33305, Taiwan, ROC
[d] Department of Nuclear Medicine and Molecular Imaging Center, Chang Gung University, Taoyuan 33305, Taiwan, ROC
[e] Department of Bioagriculture, National Chiayi University, Chiayi 60004, Taiwan, ROC

ARTICLE INFO

Article history:
Received 31 December 2015
Received in revised form
7 March 2016
Accepted 28 March 2016
Available online 31 March 2016

Keywords:
Photothermal effect
Gold nanocage
Molecular beacon
Targeted delivery
Cancer therapy

ABSTRACT

The nonspecific distribution of therapeutic agents and nontargeted heating commonly produce undesirable side effects during cancer treatment since the optimal timing of triggering the carrier systems is unknown. This work proposes a multifunctional liposomal system that can intracellularly and simultaneously deliver the therapeutic drug doxorubicin (DOX), heat, and a bubble-generating agent (ammonium bicarbonate, ABC) into targeted tumor cells to have a cytotoxic effect. Gold nanocages that are encapsulated in liposomes effectively convert near-infrared light irradiation into localized heat, which causes the decomposition of ABC and generates CO_2 bubbles, rapidly triggering the release of DOX. Additionally, a hybridized Mucin-1 aptamer is conjugated on the surface of the test liposomes, which then function as a recognition probe to enhance the uptake of those liposomes by cells, and as a molecular beacon to signal when the internalized particles have been maximized, which is the optimal time for photothermally triggering the release of the drug following the systemic administration of the liposomes. Empirical results reveal that this combined treatment effectively controls targeted drug release in a spatially and temporally precise fashion and so significantly increases the potency of the drug while minimizing unwanted side effects, making it a promising treatment for cancer.

© 2016 Elsevier Ltd. All rights reserved.

1. Introduction

Conventional chemotherapy commonly causes the nonspecific distribution of therapeutic agents, resulting in significant toxicity toward healthy tissues and limited therapeutic efficacy because the dose at the tumorigenic site is low. Molecularly targeted nanodelivery systems such as liposomes (Lips) reduce potential toxicity and enhance effective therapy [1]. To deliver the drug successfully to diseased tissues, Lips must stably encapsulate the drug in circulation but be triggered to release the contained drug after they have accumulated in the targeted cells [2]. The release of drugs from carriers can be triggered by the application of heat using a hot water bath [3], microwaves [4], or ultrasound [5]; however, such nontargeted heating frequently has adverse side effects [6]. Additionally, the optimal time for the *in vivo* heat-triggering of drug release following the systemic delivery of Lips is unknown.

This work proposes a novel Lip system that simultaneously delivers both a therapeutic agent, doxorubicin (DOX), and heat into targeted tumor cells; the DOX is rapidly released from the Lips by intracellular heat-triggering, exerting its cytotoxicity. Molecularly targeted delivery is achieved using a surface-conjugated Mucin-1 (MUC1) aptamer, which has a high binding affinity for the MUC1 protein on various tumor cells, including MCF-7 human breast cancer cells [7]. The conjugated MUC1 aptamer acts as a molecular recognition probe, and as an activatable molecular beacon following modification by hybridization with a short DNA sequence with an FITC fluorophore and a Cy3 fluorophore that are covalently attached at either terminus (FITC–MUC1 aptamer and Cy3–DNA)

* Corresponding author. Department of Chemical Engineering, National Tsing Hua University, Hsinchu 30013, Taiwan, ROC.
E-mail address: hwsung@mx.nthu.edu.tw (H.-W. Sung).
[1] The first three authors contributed equally.

http://dx.doi.org/10.1016/j.biomaterials.2016.03.040
0142-9612/© 2016 Elsevier Ltd. All rights reserved.

(Fig. 1).

In the absence of a target, the distance between the FITC fluorophore (donor) and Cy3 fluorophore (acceptor) at the end of the hybridized MUC1 (h-MUC1) aptamer is short enough to allow Förster resonance energy transfer (FRET on). However, when the aptamer binds to a target cancer cell, it can cause spontaneous conformational change, inducing dissociation of the short DNA sequence with the Cy3 fluorophore from the MUC1 aptamer with the FITC fluorophore (FRET off). Therefore, this h-MUC1 aptamer can serve as an activatable molecular beacon in an FRET-mediated alternation of a fluorescence signal, as a result of cell-membrane protein binding events (Fig. 1). This FRET imaging technique can be used to monitor the *in vivo* tumor accumulation dynamics of the h-MUC1 aptamer-conjugated Lips in real time, enabling the optimal time for the heat-triggered release of the drug following systemic administration of the test Lips to be determined.

Gold nanocages (Au NGs), ammonium bicarbonate (ABC, NH_4HCO_3, which is a CO_2 bubble-generating agent when local temperature >40 °C) [8], and DOX are encapsulated together in the aqueous core of the h-MUC1 aptamer-conjugated Lips (h-MUC1 AuNG-Lips). Upon exposure to near-infrared (NIR) light, the Au NGs generate localized heat (42 °C), which induces the decomposition of ABC, produces CO_2 bubbles, and forms permeable defects in their lipid bilayer, triggering the rapid release of DOX, increasing the intracellular drug concentration above the dose required to kill cancerous cells (Fig. 1).

2. Materials and methods

2.1. Materials

The dipalmitoylphosphatidylcholine (DPPC), cholesterol, polyethylene glycol 2000-distearoylphosphatidylethanolamine (PEG 2000-DSPE), and maleimide-functionalized PEG 2000-DSPE (Mal-PEG 2000-DSPE) were acquired from Avanti Polar Lipids (Alabaster, AL, USA), while DOX was obtained from Fisher Scientific (Waltham, MA, USA). The FITC–MUC1 aptamer and Cy3–DNA were ordered from MDBio (Taipei, Taiwan), and the anti-MUC1, anti-EEA1, and anti-LAMP2 antibodies were purchased from Abcam (Cambridge, MA, USA). All other chemicals and reagents used were of analytical grade.

2.2. Preparation of test Lips

To prepare the test Lips, DPPC, cholesterol, PEG 2000-DSPE, and Mal-PEG 2000-DSPE were dissolved in chloroform. The organic solvent was removed using a rotavapor to produce a thin lipid film (10.0 mg) on a glass vial. This film was then hydrated with Au NGs in aqueous ABC with sonication, and then underwent sequential extrusions to obtain Lips with controlled sizes. The free ABC and Au NGs were removed by dialyzing against 10 wt% sucrose solution that contained 5 mM NaCl and were then centrifuged for a short time.

To prepare test Lips that were functionalized with h-MUC1 aptamer (h-MUC1 AuNG-Lips), complementary thiol-containing FITC–MUC1 aptamer and Cy3–DNA sequence were conjugated to Mal-PEG 2000-DSPE on Lips (with a 1:1 M ratio of FITC-MUC1 aptamer/Cy3–DNA sequence:Mal-PEG 2000-DSPE) by forming a thioether linkage [9]. In the preparation of the test Lips that were functionalized with MUC1 aptamer or Cy3–DNA, only thiol-containing FITC-MUC1 aptamer or thiol-containing Cy3–DNA was conjugated to Mal-PEG 2000-DSPE on Lips (with a 1:1 M ratio of FITC-MUC1 aptamer:Mal-PEG 2000-DSPE or Cy3–DNA:Mal-PEG 2000-DSPE). The unreacted aptamer was removed by five rounds of centrifugation using a membrane ultrafiltration filter tube (Vivaspin 2, MWCO: 3 kDa; GE Healthcare, Buckinghamshire, UK).

Subsequently, DOX was mixed with the h-MUC1 AuNG-Lip suspensions with a 0.05 drug/lipid weight ratio and maintained

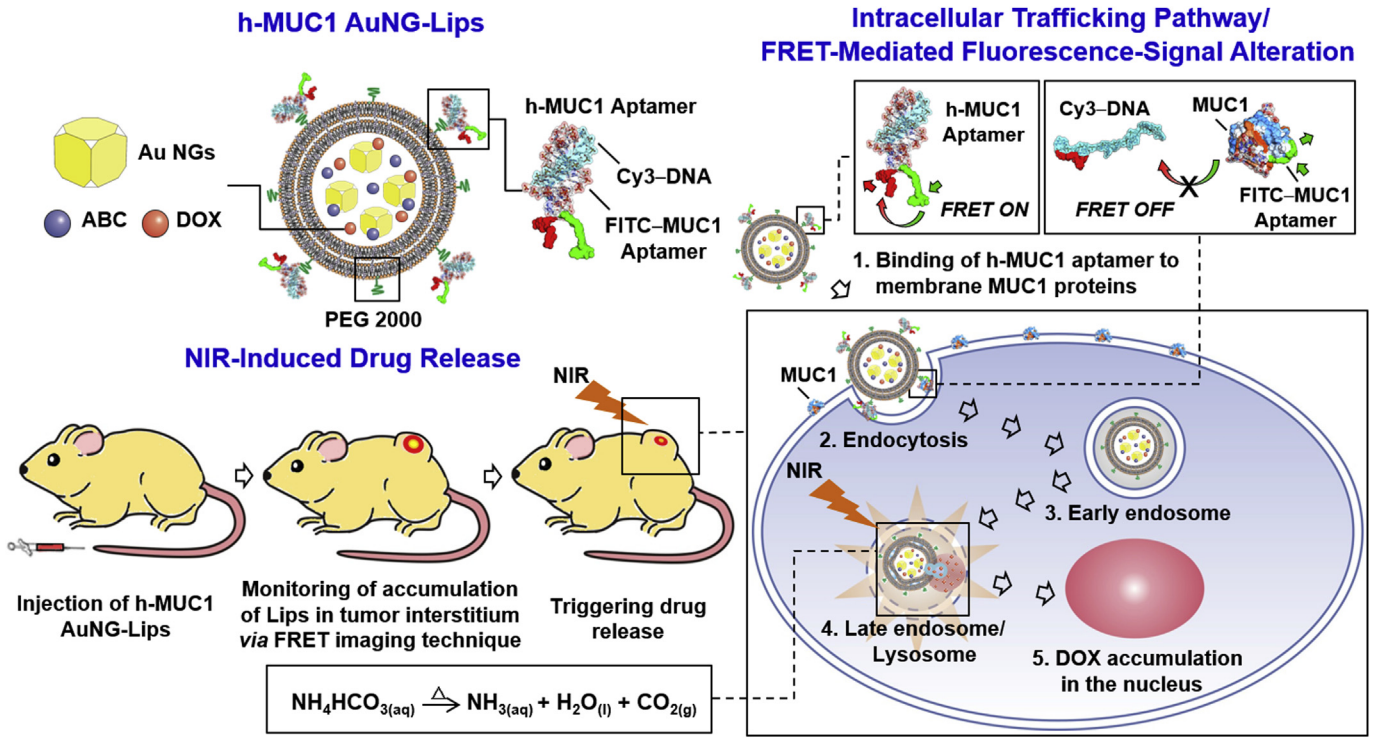

Fig. 1. Composition and structure of an h-MUC1 AuNG-Lip, and its mechanism of simultaneous delivery of heat and DOX into a tumor cell for spatially and temporally precise targeted drug delivery.

at room temperature for 24 h. Finally, the Lips were passed through a G-50 column (GE Healthcare, Buckinghamshire, UK) to eliminate the unencapsulated DOX. It has been reported that DOX may bind with aptamer through a weak van der Waals force [10]. Mechanical stirring with sonication was therefore used to eliminate the possibility of the physical entanglement of DOX on the as-prepared Lips.

2.3. Characterization of test Lips

The mean particle size and zeta potential of the as-prepared Lips were measured by dynamic light scattering (Zetasizer 3000HS; Malvern Instruments, Worcestershire, UK), while the DOX encapsulation efficiency and content were determined by making fluorescence measurements (Spex FluoroMax-3; Horiba Jobin Yvon, Edison, NJ, USA) after the test Lips had been destroyed using Triton X-100. The encapsulation efficiency was the mass of DOX in Lips divided by the mass of DOX in the initial solution × 100%.

The thermoresponsive characteristics of the test Lips were elucidated by examining the formation of CO_2 bubbles in a test tube that contained the Lips in phosphate-buffered saline (PBS, pH 7.4) at 37 or 42 °C (w/o or w/NIR exposure). The test tubes that contained the samples were immersed in a water-filled tank, and the formation of CO_2 bubbles was studied using an ultrasound imaging system (Z-one, Zonare; Mountain View, CA, USA).

The *in vitro* DOX release profiles were obtained by immersing the test Lips (10 mg/mL, 50 μL) in quartz cells that contained 1 mL PBS, which were gently shaken in a thermostatic rotary shaker at 100 rpm and 37 °C. Aqueous suspensions of h-MUC1 AuNG-Lips at 42 °C were irradiated from above using an NIR laser (808 nm, Tanyu Tech., Taiwan) with a power density of 0.8 W/cm^2. An infrared (IR) thermal camera (PV320, Electrophysics, Fairfield, NJ, USA) was placed above the suspension to capture the temperature of the bulk solution. Samples were removed at predetermined intervals and upon each removal, an equal amount of the same medium was added to maintain a constant volume. The amount of DOX that was released from the test Lips was analyzed using fluorescence spectrometry.

2.4. Molecular dynamic (MD) simulations

The MD simulations of the interaction between the h-MUC1 aptamer and the MUC1 protein were performed using a previously described method [11]. Images of the molecules with atomic detail were generated in UCSF Chimera software [12].

2.5. Internalization of test Lips

To quantify the cellular uptake of test Lips, MCF-7 human breast cancer cells were plated in 12-well plates at 2 × 10^5 cells/well and co-cultured with the 3,3′-dioctadecyloxacarbocyanine perchlorate (DiO)-labeled Lips (without the conjugation of FITC and Cy3) at 10 μg/mL for various incubation times. Following incubation, cells were detached by 0.025% trypsin/ethylenediaminetetraacetic acid (EDTA) and transferred to microtubes. Then, the cells were resuspended in PBS that contained 1 mM EDTA and 2% fetal bovine serum and fixed in 4% paraformaldehyde. Finally, cells were analyzed using a flow cytometer that was equipped with a 488 nm argon laser (Beckman Coulter, Fullerton, CA, USA).

2.6. Intracellular trafficking

Following incubation with DiO-labeled Lips, cells were washed twice in PBS before they were fixed in 4% paraformaldehyde. The fixed cells were studied using immunohistochemical staining to identify the MUC1 protein, endosomes (EEA1), and lysosomes (LAMP2) and they were counterstained using DAPI to visualize the nuclei, before being examined by a confocal laser scanning microscope (CLSM, Zeiss LSM780, Carl Zeiss, Jena GmbH, Germany).

2.7. Intracellular accumulation of DOX

To evaluate intracellular DOX accumulation, MCF-7 cells were treated with test Lips in a serum-free medium. Following incubation, the cells were washed twice in pre-warmed PBS and then fixed in 4% paraformaldehyde. The intracellular accumulation of DOX was qualitatively examined using CLSM and quantified by flow cytometry.

2.8. Cell viability assay

The MCF-7 cells were co-cultured with test Lips for 30 min. Following NIR irradiation, samples were aspirated and cells were incubated in a medium that contained 1 mg/mL MTT [3-(4,5-dimethylthiazol-2-yl)-2,5-diphenyltetrazolium bromide] reagent for 4 h; 1 mL dimethyl sulfoxide (DMSO) was then added. Optical density readings were obtained using a multi-well scanning spectrophotometer (Dynatech Laboratories, Chantilly, VA, USA).

2.9. In vitro FRET dual-emission fluorescence

MCF-7 cells were plated in 96 well plates at 5 × 10^4 cells/well and co-cultured with h-MUC1 AuNG-Lips at 10 mg/mL; suspensions of Lips that were conjugated with the FITC–MUC1 aptamer, Cy3–DNA, or h-MUC1 aptamer were the controls. To avoid the fluorescence interference, the test Lips containing no DOX were used in this specific experiment. Fluorescence images over time were obtained using an *in vivo* imaging system (IVIS). Test samples were excited at a donor excitation wavelength of 500 nm; FITC and Cy3 images were then acquired through 520 nm and 560 nm emission filters, respectively. Fluorescence intensities in a region of interest of tumors were quantified using Living Image software.

2.10. In vivo FRET molecular imaging

MCF-7 cells were injected subcutaneously into the left flank of BALB/c nude mice. When the tumor size reached around 100 mm^3, 8 h-fasted nude mice (n = 3) were anesthetized and *i.v.* injected with h-MUC1 AuNG-Lips that did not contain DOX (10 mg/mL, 350 μL). The tumors were irradiated at an excitation wavelength of 500 nm, and fluorescence images were acquired in the Cy3 emission channel of 560–640 nm before *i.v.* injection, 15 min, 30 min, 1 h, 1.5 h, and 2 h after injection using an IVIS. The tissue autofluorescence and the Cy3 fluorescence were then unmixed by the Living Image software package [13].

2.11. Animal study

BALB/c nude mice (6–8 weeks old) were obtained from the National Laboratory Animal Center, Taiwan. All animal experiments were consisted with the “Guide for the Care and Use of Laboratory Animals” of the Institute of Laboratory Animal Resources, National Research Council, published in 1996 by the National Academy Press. The Institutional Animal Care and Use Committee of National Tsing Hua University approved the study protocol (no. 10258). A Matrigel (BD Biosciences, Franklin Lakes, NJ) that contained 5 × 10^6 MCF-7 cells was subcutaneously injected using a 26-gauge needle into the left flank of each nude mouse and grown to a volume of 100–150 mm^3 [14].

2.12. In vivo DOX accumulation

Free DOX and h-MUC1 AuNG-Lips were individually injected intravenously into the tail vein of mice with MCF-7 tumors (n = 6 for each studied group). To avoid the fluorescence interference with the DOX emission signal, the h-MUC1 AuNG-Lips that were not labeled by FITC and Cy3 were used in this specific study. Photothermal treatment by NIR irradiation (~1.2 W/cm^2) was conducted on the group that had received h-MUC1 AuNG-Lips at 1 h following administration. Four hours after treatment, the mice were sacrificed, and their organs and tumors were harvested and visualized using an IVIS imaging system. The harvested tissues were irradiated at 500 nm, which is the excitation wavelength of DOX (485 ± 15 nm); the fluorescence images were then acquired through a 580 nm-emission filter. An aqueous solution of deionized water and ethanol was then added to each test tissue. The mixture was then homogenized and centrifuged; the supernatant was lyophilized and resuspended in deionized water. Finally, the fluorescence intensity of the solution was measured using a spectrofluorometer (F-2500; Hitachi, Tokyo, Japan).

2.13. Antitumor efficacy

Test mice were divided into four groups and each mouse was injected intravenously in the tail under one of the following experimental conditions; saline, free DOX, h-MUC1 AuNG-Lips w/o NIR exposure, and h-MUC1 AuNG-Lips w/NIR exposure (n = 6 per group). The dose of DOX under each test condition was 2 mg per kg body weight four times, once every four days. The tumor size and body weight of each mouse were measured every other day and normalized to their initial values. Tumor size was estimated using a pair of calipers, and tumor volume was calculated as $V = (\pi/6) \times LW^2$, where L and W are the long and short diameters, respectively [15].

At the end of the treatment, the mice fasted overnight were then anesthetized using isoflurane (2% in 100% O_2), before 11.7 ± 0.2 MBq ^{18}F-FDG (2-deoxy-2-[fluorine-18]fluoro-D-glucose) in 100 μL of saline was injected into their tail veins. A 10 min image acquisition using a positron emission tomography (PET) scanner was carried out one hour after ^{18}F-FDG administration (Siemens Medical Solutions, Knoxville, TN, USA). Following PET scanning, x-ray computerized tomography (CT) images were obtained using NanoSPECT/CT (Bioscan, Washington, DC, USA) [16]. Finally, the mice were sacrificed, and tissue samples were sectioned and stained with hematoxylin and eosin stain (H&E) for histological observation. The apoptosis of tumor cells was determined using the TUNEL (terminal deoxynucleotidyl transferase dUTP nick end labeling) assay, following the manufacturer's instructions (Roche Diagnostics GmbH, Mannheim, Germany).

2.14. Statistical analysis

Pairs of groups were compared using the one-tailed Student's *t*-test in statistical software (SPSS, Inc., Chicago, IL, USA). Sets of more than two groups were compared by One-way ANOVA followed by the Bonferroni post hoc test. Data are presented as mean ± standard deviation. Differences were considered to be statistically significant when $P < 0.05$.

3. Results and discussion

3.1. Characteristics of test Lips

A Lip-based carrier is one of the most common drug delivery systems. The proposed Lip formulation consisted of DPPC, cholesterol, PEG 2000-DSPE, and Mal-PEG 2000-DSPE in a 60:40:2.5:2.5 M ratio [17]. The Au NGs were fabricated *via* a galvanic replacement reaction between Ag nanocubes and $HAuCl_4$, based on a protocol in the literature [18]. The as-prepared Au NGs exhibited pronounced surface plasmon resonance (SPR) absorption in the NIR region at 780 nm (Fig. 2a), with an outer edge length of 45.3 ± 4.2 nm and an inner edge length of 35.1 ± 2.4 nm (n = 10 batches, Fig. S1a).

The test Lips were prepared at room temperature by the lipid film hydration technique followed by sequential extrusion [19,20]. The Au NGs (0.5, 1.0, or 2.0 nM) and saturated ABC (2.7 M) were incorporated into the aqueous compartment of the Lips when suspensions were formed by lipid hydration. Generally speaking, the final internal and external concentrations of the as-prepared liposomes would be equal [21]. The thiol-modified h-MUC1 aptamer was subsequently conjugated with Mal-PEG 2000-DSPE on the Lips. Efficient loading of DOX (90.8 ± 6.7%, n = 6 batches) into the aqueous phase of the Lips (h-MUC1 AuNG-Lips) was achieved by exploiting the transmembrane gradient of ABC [22]. The concentration of DOX that was encapsulated in the Lips (approximately 0.045 mg DOX per mg lipids) was about 100 times its saturated concentration at room temperature. The hydrodynamic size and zeta potential of the as-prepared Lips were 215.2 ± 22.2 nm and −7.2 ± 0.5 mV, respectively.

3.2. Optical properties and photothermal effects of test Lips

Encapsulation in the test Lips red-shifted the SPR absorption peak of Au NGs from 780 to 810 nm by reducing their interparticle distance, and increased their bandwidth above that of Au NGs alone (Fig. 2a). The stable encapsulation of Au NGs in the resultant Lips was verified by obtaining transmission electron microscopy (TEM) images (Fig. S1b).

To elucidate their photothermal effects, aqueous suspensions of h-MUC1 AuNG-Lips were exposed to an NIR laser, and an IR thermal camera was used to record their bulk solution temperatures. NIR irradiation at 808 nm rapidly increased the bulk temperatures of suspensions of h-MUC1 AuNG-Lips, which plateaued at their maximum values within 5 min (Fig. 2b); this effect was accompanied by gas-bubble generation (Fig. 2c), as the heating decomposed the ABC to CO_2 gas, water, and ammonia [23,24]. The rate of increase in temperature and the final bulk temperature were proportional to the amount of Au NGs that were encapsulated within the test Lips. The Au NGs, which can absorb considerable NIR light and convert it into heat, have been studied for use as heat carriers [25]. This heating is efficient and highly localized because the temperature change is mostly limited to the region around the Au NGs. However, one of the restrictions for NIR irradiation is its penetration depth (approximately 3 cm in biological tissues [26]), thus limiting the technique developed in the study applicable only for superficial tumors.

In this work, the aim is to limit the local temperature to ≤42 °C to prevent damage to surrounding tissues. When tissues are heated to >45 °C, cells typically undergo apoptosis or mitotic death [27]. Therefore, test Lips with 1.0 nM Au NGs, which had a local temperature of 42 °C, were used in the subsequent experiments.

3.3. In vitro drug release profiles

Fig. 2d presents the *in vitro* DOX release profiles from suspensions of h-MUC1 AuNG-Lips at a bulk temperature of 37 or 42 °C. The DOX release profiles were obtained by measuring increases in the fluorescence intensities of the suspensions in PBS over time. The bulk temperature of 37 °C for h-MUC1 AuNG-Lip suspensions was maintained using a circulating water bath,

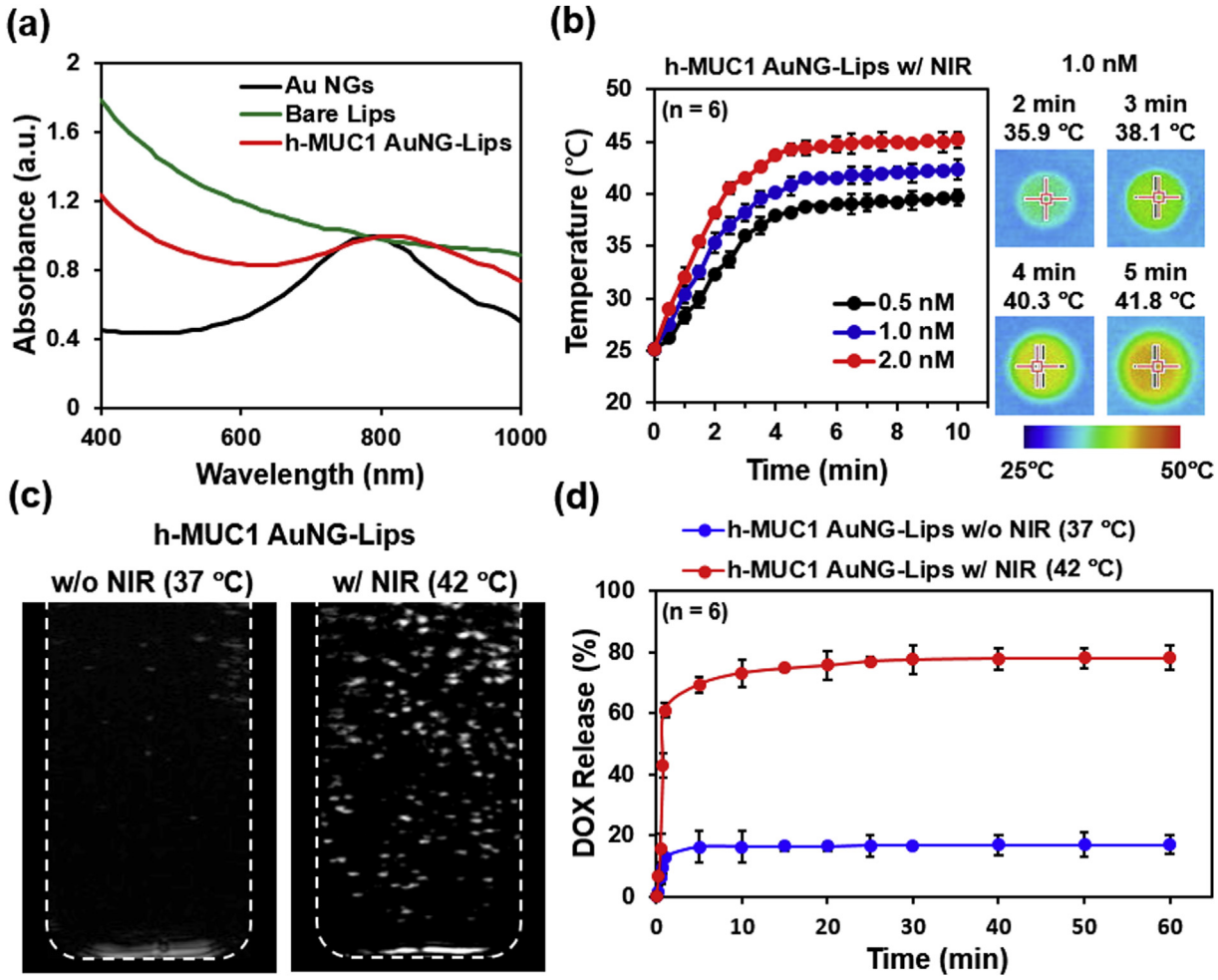

Fig. 2. (a) Light absorption spectra of suspensions of Au NGs, bare Lips, or h-MUC1 AuNG-Lips. (b) Temperature vs. irradiation time profiles and corresponding thermographic images of suspensions of h-MUC1 AuNG-Lips that were formulated with Au NG concentrations of 0.5, 1.0, or 2.0 nM (n = 6). (c) Ultrasound images of h-MUC1 AuNG-Lip suspensions, formulated with an Au NG concentration of 1.0 nM at a bulk temperature of 37 °C (w/o NIR exposure) or 42 °C (w/NIR exposure). (d) Release profiles of DOX from h-MUC1 AuNG-Lips that were incubated at a bulk temperature of 37 °C or 42 °C (n = 6).

while the bulk temperature of 42 °C was maintained by irradiation under an NIR laser. Relatively small amounts (17 ± 3%) of DOX were released from h-MUC1 AuNG-Lip suspensions at 37 °C. When the bulk temperature was increased to 42 °C under NIR, significant amounts of encapsulated DOX were instantaneously released from the test Lips (78 ± 4%). This release was photothermally triggered by the internal generation of CO_2 bubbles during ABC decomposition (Fig. 2c), rather than *via* direct heating of the test liposomes since their transition temperature was approximately 52 °C [17].

3.4. FRET-mediated fluorescence-signal alteration

Fig. S2 presents the FRET spectra of aqueous FITC–MUC1 aptamer, Cy3–DNA, h-MUC1 aptamer (hybridized Cy3–DNA/FITC–MUC1 aptamer), and the negative control (in which the Cy3–DNA sequence was fully uncomplementary to the FITC–MUC1 aptamer, and is referred to as uh-MUC1 aptamer). All spectra were obtained by irradiating test samples at 485 nm, which is the excitation wavelength of the FRET donor, FITC (500 ± 15 nm). Among all of the test samples, only the h-MUC1 aptamer exhibited significant FRET behavior (as indicated by black arrows); specifically, the intensity of FITC decreased greatly while that of Cy3 increased significantly, suggesting that its DNA sequence and MUC1 aptamer were well complementary.

3.5. MD simulations

MD simulations were performed using a full-atom model to identify the mechanism by which the h-MUC1 aptamer functions as an activatable molecular beacon in the presence of MUC1 protein, which is a transmembrane protein that is overexpressed in almost all human epithelial cell adenocarcinomas [28]. When lacks a target, hybridization of the DNA sequence with its complementary part of the MUC1 aptamer causes the distance between the terminal Cy3 fluorophore (acceptor) and FITC fluorophore (donor) to be small (approximately 3 nm), so energy is transferred between the two dyes (FRET on), suppressing fluorescence of the reporter dye (FITC, Fig. 3a). Conversely, when encountering a target, the h-MUC1 aptamer binds with the MUC1 protein, causing its spontaneous conformational reorganization, forcing the quencher dye (Cy3–DNA) to separate and move far from the reporter dye (FITC–MUC1 aptamer, >10 nm; Supplementary Video 1), ultimately increasing reporter fluorescence (FRET off). This method is an extension of the use of the well-known molecular beacons, based on the FRET principle, to control fluorescence emission when they interact with well-defined molecular targets [29].

Supplementary data related to this article can be found online at

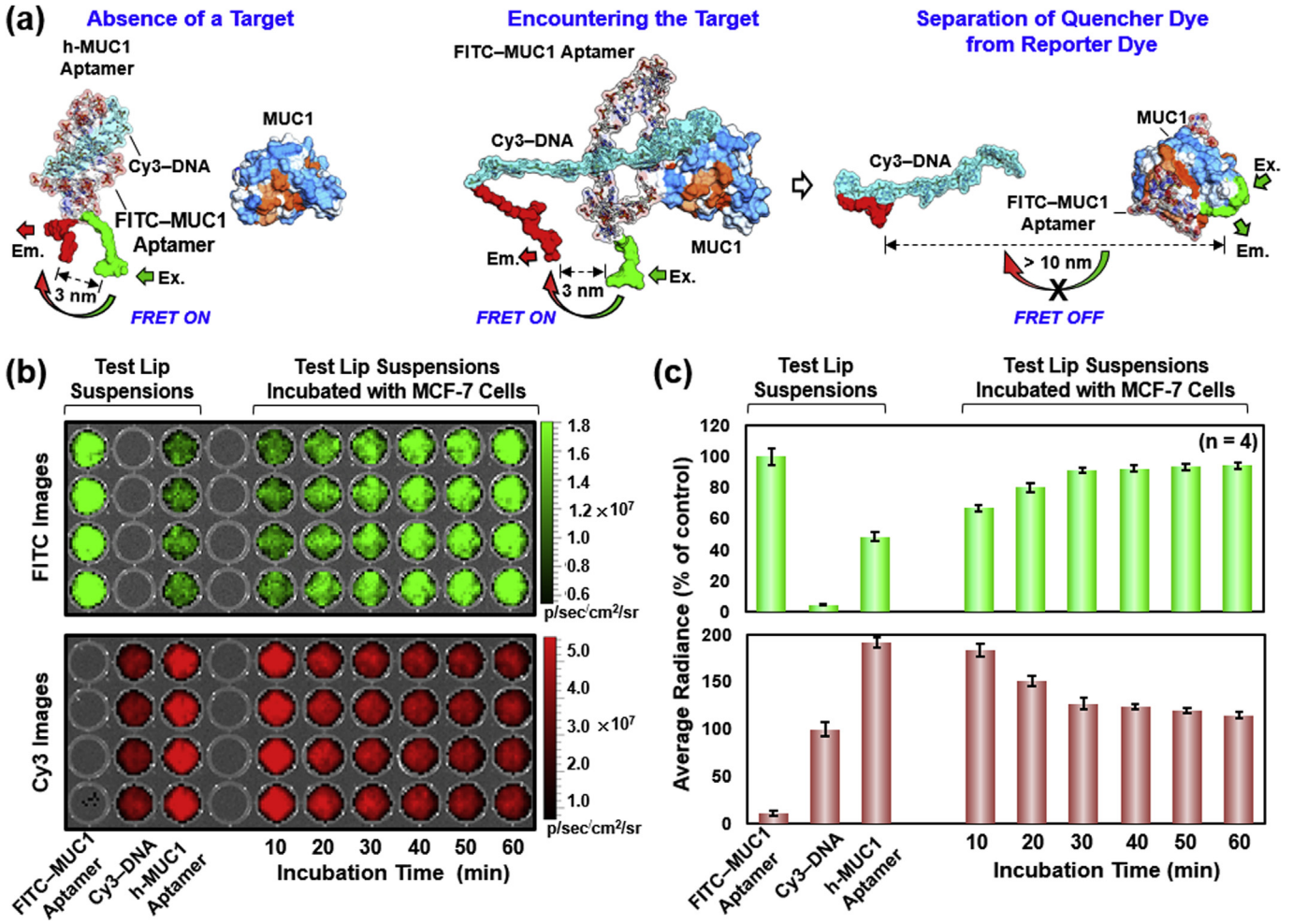

Fig. 3. (a) MD simulation results concerning interaction between h-MUC1 aptamer and MUC1 protein. (b) Dual-emission images and (c) corresponding fluorescence intensities of MCF-7 cells incubated with h-MUC1 AuNG-Lips, obtained using an IVIS (n = 4); suspensions of Lips conjugated with FITC–MUC1 aptamer, Cy3–DNA, or h-MUC1 aptamer were controls.

http://dx.doi.org/10.1016/j.biomaterials.2016.03.040.

3.6. *In vitro FRET dual-emission fluorescence*

Fig. 3b and c present dual-emission images and their corresponding fluorescence intensities of MCF-7 cells that were incubated with h-MUC1 AuNG-Lips. Suspensions of Lips that were conjugated with the FITC–MUC1 aptamer, Cy3–DNA, or h-MUC1 aptamer were the controls. Following incubation with MCF-7 cells, the fluorescent intensity of the FITC band (green) of the h-MUC1 AuNG-Lips increased over time, while that of the Cy3 band (red) declined gradually (Fig. 3b). Notably, the reduction of FITC FRET-mediated Cy3 emission became negligible following 30 min of incubation (Fig. 3c), suggesting that the number of h-MUC1 AuNG-Lips that bind to target cancer cells *via* the MUC1-receptor had peaked. The bound Lips may then be able to enter the tumor cells through the specific MUC1-mediated endocytosis pathway [30]. In receptor-mediated endocytosis, the number of drug carriers that can be internalized into cells is likely to be maximized when their surface receptors for carriers are saturated [31].

3.7. *Internalization of test Lips*

To determine whether the h-MUC1 aptamer can differentially bind to MUC1-expressing cancer cells, the DiO-labeled Lips were separately incubated with MCF-7 (MUC1-postive) and HepG2 (a MUC1-negative human hepatic cancer cell line) cells [7]. Following incubation for specific periods, the cells were analyzed by flow cytometry; those treated with bare Lips or MUC1 AuNG-Lips were used as controls.

The bare Lips were not preferentially taken up by either MUC1-positive or MUC1-negative cells nor did they exhibit higher fluorescence intensity in those cells ($P > 0.05$), probably because the mechanisms of the uptake of bare Lips by both cell lines are similar. In contrast, the MUC1 AuNG-Lips generated a markedly more potent cellular uptake/fluorescence signal in MUC1-postive cells than in MUC1-negative cells ($P < 0.05$), revealing that the MUC1 aptamer can discriminate between target and non-target cells. h-MUC1 AuNG-Lips exhibited similar binding preferences to the test cell lines as did MUC1 AuNG-Lips ($P > 0.05$). This similarity strongly suggests that the h-MUC1 aptamer retains its selectivity and can bind specifically to cancer cells that overexpress MUC1 protein and significantly improve their endocytotic internalization. The use of a targeting moiety promotes internalization of the carriers by switching the mechanism of internalization from simple endocytosis to receptor-mediated endocytosis [32]. Notably, fluorescence intensity within MCF-7 cells peaked at approximately 30 min following incubation (Fig. 4a), indicating that the number of internalized Lips was maximized, verifying the concept that was anticipated in the above dual-emission imaging study (Fig. 3c).

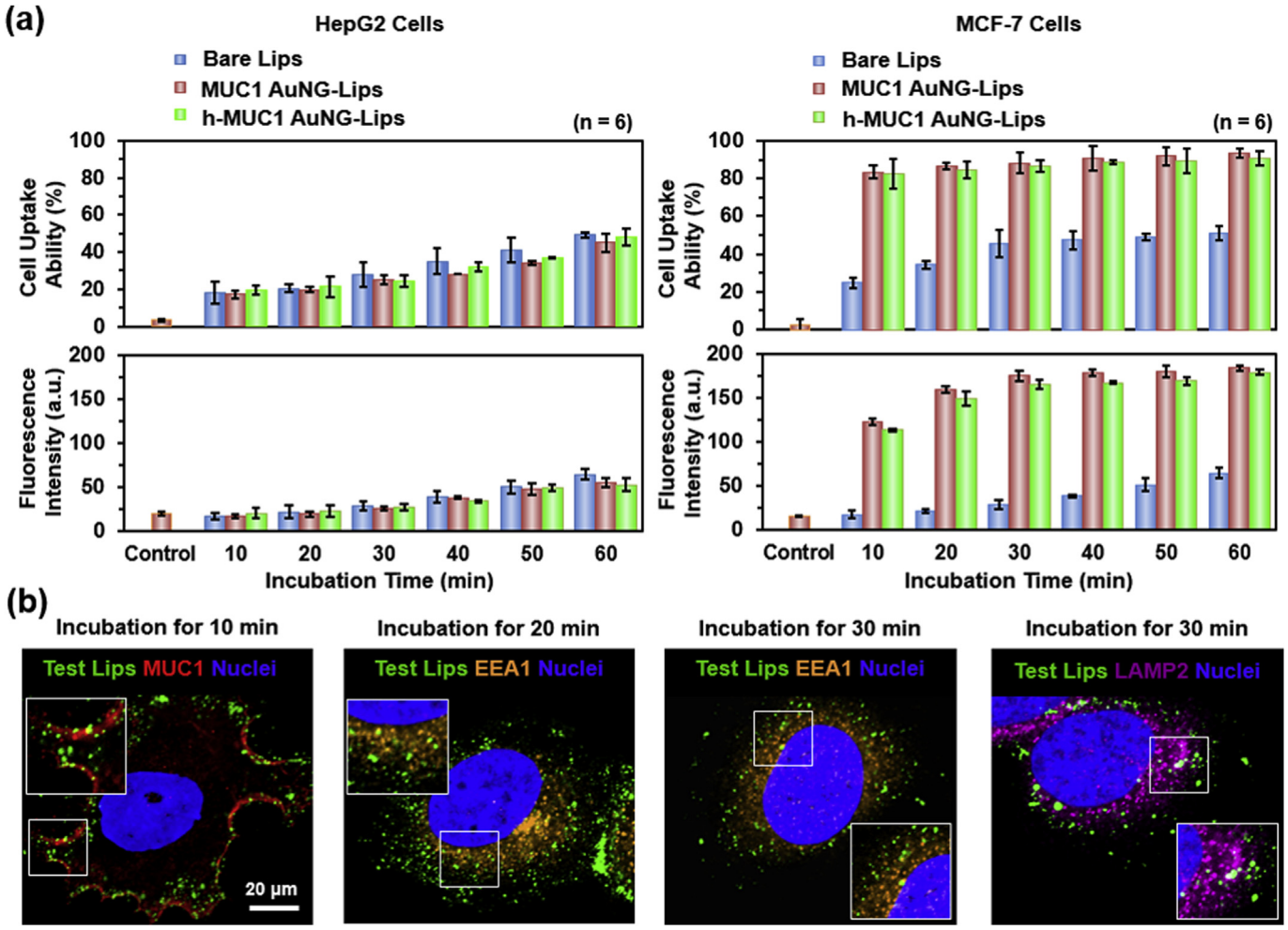

Fig. 4. (a) Flow-cytometry results concerning cellular uptake of h-MUC1 AuNG-Lips in HepG2 (MUC1-negative) and MCF-7 (MUC1-postive) cells (n = 6). (b) CLSM images at indicated times, showing intracellular trafficking of internalized h-MUC1 AuNG-Lips.

3.8. Intracellular trafficking

Intracellular trafficking of internalized Lips was studied by the potential co-localization of test particles and intracellular organelles using CLSM. Ten minutes after incubation, the DiO-labeled Lips (green) exhibited high co-localization with the MUC1 protein (stained red with the anti-MUC1 antibody) on the plasma membrane of target MCF-7 cells (Fig. 4b). At 20 min, a significant number of Lips were co-localized with early endosomes (stained orange with the anti-EEA1 antibody). After 30 min of incubation, the early endosomes matured into late endosomes/lysosomes (stained purple with the anti-LAMP2 antibody), which are typically located close to the nuclei. The DOX must be transported into the nuclei to interact with DNA by the intercalation and inhibition of macromolecular biosynthesis to have its cytotoxic effect [33]. The release of DOX in the vicinity of the cell nuclei has been suggested to improve the efficacy of the drug by reducing its diffusion distance [2]. Consequently, the photothermally triggered release of DOX from the test Lips under NIR exposure for 10 min was initiated 30 min after cell incubation in the following experiments.

3.9. Intracellular accumulation of DOX and cell viability

Following NIR irradiation, the intracellular accumulations of DOX that had been released from the internalized Lips were visualized qualitatively by CLSM (Fig. 5a) and quantified by flow cytometry (Fig. 5b). The MTT assay was used to assess their cytotoxicity toward MCF-7 cells (Fig. 5c). As compared to untreated cells (Control, Fig. 5a and b) at a bulk temperature of 37 °C, the nuclei of MCF-7 cells that were treated with h-MUC1 AuNG-Lips alone (unexposed to NIR light) had weak red fluorescence, indicating the presence of DOX; consequently, the number of cells that were killed by the test Lips was minimal (8%). Approximately 20% of cells were killed with the combined treatment of h-MUC1 AuNG-Lips (containing no DOX) and NIR light heating, owing to the highly localized heat generated by the Au NGs that were encapsulated in the test Lips. In experiments at a bulk temperature of 42 °C with NIR irradiation, the DOX accumulation in the nuclei was much stronger (Fig. 5a and b, $P < 0.05$) so the toxicity toward MCF-7 cells was much higher (with 55% of cells killed, $P < 0.05$, Fig. 5c). The higher cell killing effectiveness is probably attributable to the fact that the target cells were heated by the laser, promptly triggering the release of DOX from the internalized Lips (Fig. 2d), making it bioavailable. Additionally, heat has been used to improve the efficacy of chemotherapy [6,34].

3.10. In vivo FRET molecular imaging

Based on the above *in vitro* results, the effective intracellular release of a drug from internalized h-MUC1 AuNG-Lips within

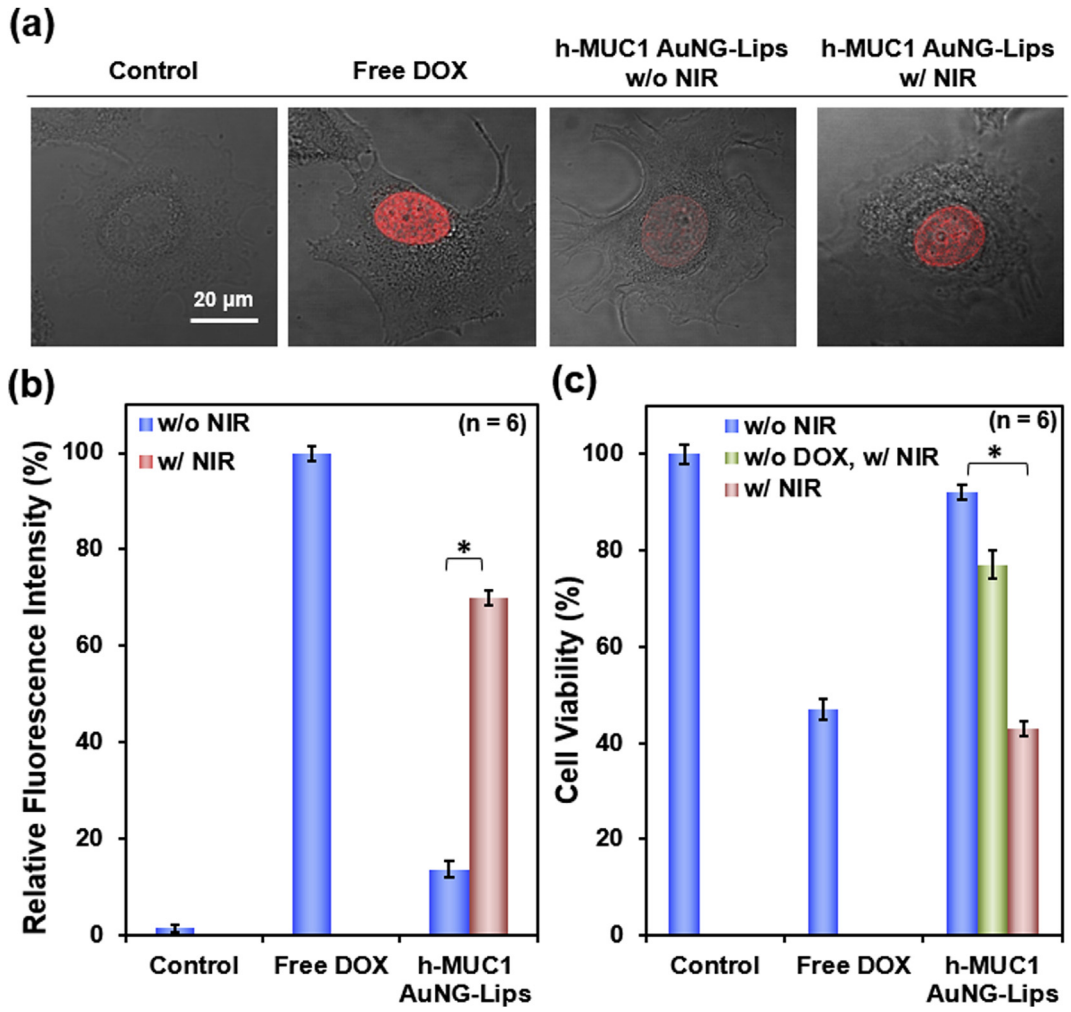

Fig. 5. (a) CLSM images and (b) flow-cytometry results concerning intracellular accumulation of DOX in MCF-7 cells that were treated with free DOX or h-MUC1 AuNG-Lips (20 μM DOX in each group) at a bulk temperature of 37 °C (w/o NIR exposure) or 42 °C (w/NIR exposure), and (c) cell viability of MCF-7 cells, as determined by MTT assay (n = 6). *Statistical significance indicated by $P < 0.05$.

defined spatial and temporal ranges is a prerequisite for improved *in vivo* therapeutic efficacy. Systemically administered nanosized carriers must flow through the vasculature towards the tumor, be transported across vascular walls *via* the enhanced permeability and retention (EPR) effect [35], and move through the interstitium. Additionally, the successful intracellular delivery of carriers that contain an entrapped drug depends on their specific binding with cellular receptors, followed by internalization. Premature loss of drug content before receptor-mediated uptake of the carriers prevents any anti-tumor effects [36]. Accordingly, to maximize the *in vivo* therapeutic efficacy of the drug content, the dynamics of carrier accumulation at the tumorigenic site and the time of triggering the drug release from the internalized carriers must be known.

The dynamics of the accumulation of dual-labeled h-MUC1 AuNG-Lips at the tumor interstitium and their subsequent binding to the MUC1 receptors on the surfaces of tumor cells were investigated upon their intravenous (IV) administration, based on FRET principles. BALB/c nude mice with a subcutaneous MCF-7 tumor on their left flank were used as an animal model. The tumors were irradiated at a wavelength of 500 nm (which is the excitation wavelength of FITC), and molecular fluorescence images were captured in the optical window of 560–640 nm (Cy3 emission channel) using an IVIS. The Living Image software package was used to unmix the native tissue autofluorescence and the Cy3 fluorescence to obtain images of unmixed Cy3.

FRET is a very efficient quencher of fluorescence. As demonstrated above (Fig. 3), before the dual-labeled h-MUC1 AuNG-Lips were bound to the MUC1 receptors on MCF-7 cells, the hybridization distance between their Cy3–DNA sequence and the complementary FITC–MUC1 aptamer on the test Lips was short enough for FRET energy transfer (FRET on), so the quencher dye (Cy3) fluoresced. Following their binding to the target cells, the Cy3–DNA was forced to dissociate from the FITC–MUC1 aptamer (FRET off), dequenching the Cy3 emission (Fig. 3).

The results in Fig. 6 suggest that upon IV administration, the Cy3 emission from the tumor was elevated, indicating the accumulation of h-MUC1 AuNG-Lips in the tumor *via* the EPR effect. The strength of the FRET signal became maximal approximately 30 min after IV administration, suggesting that the number of test Lips that accumulated at the tumor interstitium had peaked. Thereafter, the Cy3 signal that was emitting from the tumor began to decline, vanishing over time, probably owing to the dissociation of Cy3–DNA from the Lips after they bind to the MUC1 receptors on target MCF-7 cells. These experimental results reveal that the FRET imaging technique developed herein allows us to monitor the dynamics of the accumulation of test Lips in the tumor and their binding to the target cells, providing a means of molecular imaging and optically

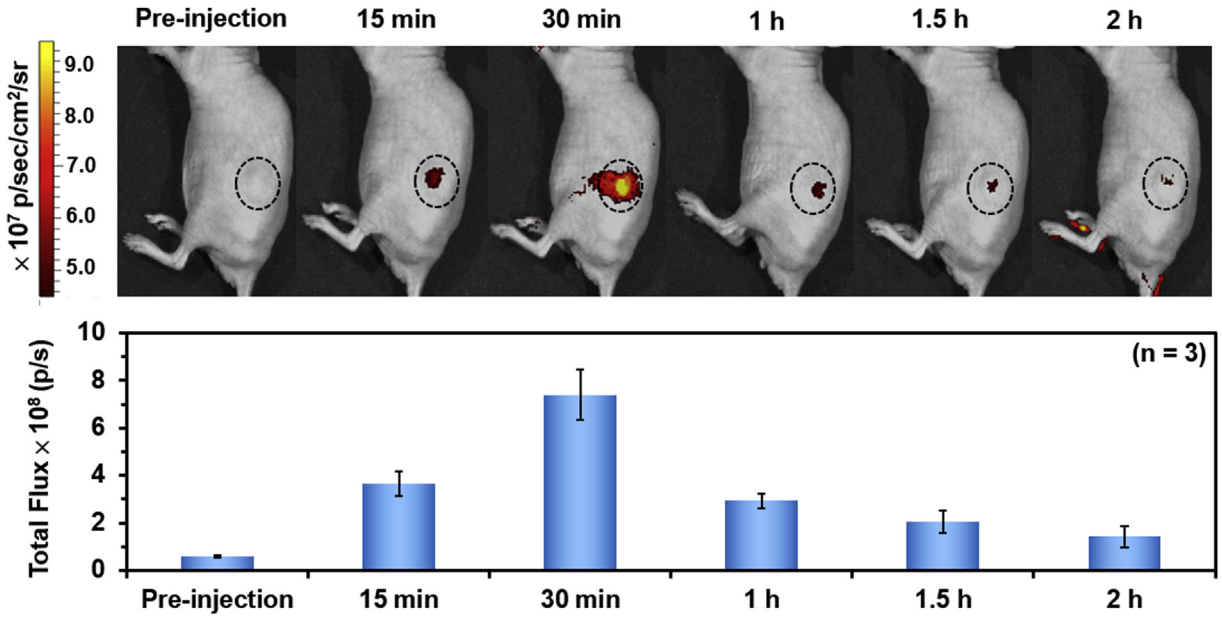

Fig. 6. Time-dependent fluorescence Cy3 images and corresponding intensities following intravenous injection of h-MUC1 AuNG-Lips into tail vein of mice with MCF-7 tumors, revealing dynamics of tumor accumulation of test Lips and their binding to target cells.

visualizing the *in vivo* behavior of drug carriers in real time. However, owing to the rapid attenuation of light in tissues, the FRET signal is relatively weak, and therefore this approach is likely to be useful only for superficial tumors.

After binding to the tumor cells, the ligand-targeted Lips that contained entrapped DOX entered the endosomal/lysosomal compartments of those cells *via* receptor-mediated endocytosis. Based on the *in vitro* results (Fig. 4a), the number of h-MUC1 AuNG-Lips that were internalized into MCF-7 cells reached its peak approximately 30 min after incubation. The internalized Lips only become bioavailable when their entrapped drug is released [36]. The release of the drug from the internalized Lips, which can be triggered photothermally upon exposure to the NIR laser for 10 min (Fig. 5a and b), is therefore initiated 1 h after the tail-vein injection (calculated as 30 min to the maximum accumulation of the test Lips at the tumor interstitium plus 30 min to their maximum internalization) in the following animal studies.

3.11. *In vivo photothermal effects*

Effectiveness of the h-MUC1 AuNG-Lips that accumulated at the tumor site in converting NIR light energy into local heat was monitored using an IR thermal camera. The tumors treated with test Lips alone or receiving NIR only and that without any treatment (empty control) were used as controls. Similar to the empty control (Fig. 7a), no significant change in temperature occurred at the tumor site (with a skin surface temperature of approximately 29 °C) for the group that received only test Lips. Meanwhile, the temperature of the tumor that was exposed to NIR light (~1.2 W/cm^2) alone increased slightly to about 31 °C. Conversely, the temperature of the tumor that was treated with test Lips and NIR exposure (w/NIR) increased to 42 °C, implying an excellent photothermal capacity of the accumulated h-MUC1 AuNG-Lips upon activation by the NIR laser.

3.12. *In vivo DOX accumulation*

This study also investigated how local photothermal treatment affects the amount of DOX that is released from h-MUC1 AuNG-Lips that have accumulated in tumors. Test Lips were injected intravenously into the tail vein of mice that bore MCF-7 tumors; at 1 h after administration, the tumor site was heated to 42 °C by NIR exposure (h-MUC1 AuNG-Lips w/NIR) for 10 min before being allowed to cool for 5 min; this process was carried out three times in immediate succession. The group without NIR treatment (h-MUC1 AuNG-Lips w/o NIR) and the group that had received free DOX were the controls. Four hours following the treatment, the mice were sacrificed, and their organs (including the tumors) were harvested. The accumulation of DOX in tissues was examined by an IVIS, and their fluorescence intensities thereof were quantified using a spectrofluorometer.

As presented in Fig. 7b and c, the tumors that had received free DOX yielded a weak DOX fluorescence signal, owing to its inherently low selectivity. The tumors in the groups that had been treated with h-MUC1 AuNG-Lips exhibited significantly stronger DOX signals – especially when heated locally under NIR irradiation ($P < 0.05$). These findings demonstrate that h-MUC1 AuNG-Lips were successfully delivered to the tumor tissues *via* the EPR effect and internalized by receptor-mediated endocytosis (Fig. 4). Triggering by NIR light of the generation of localized heat (42 °C) by encapsulated Au NGs decomposed the ABC and facilitated the immediate thermal formation of CO_2 bubbles (Fig. 2c), promoting intracellular release and the accumulation of DOX (Fig. 5a and b). Only the hearts that had received free DOX yielded a detectable DOX signal. The non-specific selectivity of DOX may be responsible for its systemic toxicity toward healthy tissues and prevent the use of high doses that are effective in killing cancer cells, limiting its clinical use [32].

3.13. *Antitumor efficacy*

The therapeutic efficacy of the above formulations in suppressing the growth of tumors in nude mice was studied using the same procedure as in the above study of *in vivo* DOX accumulation. The group that was treated with saline served as an empty control. According to Fig. 8a, the antitumor activity of the group that

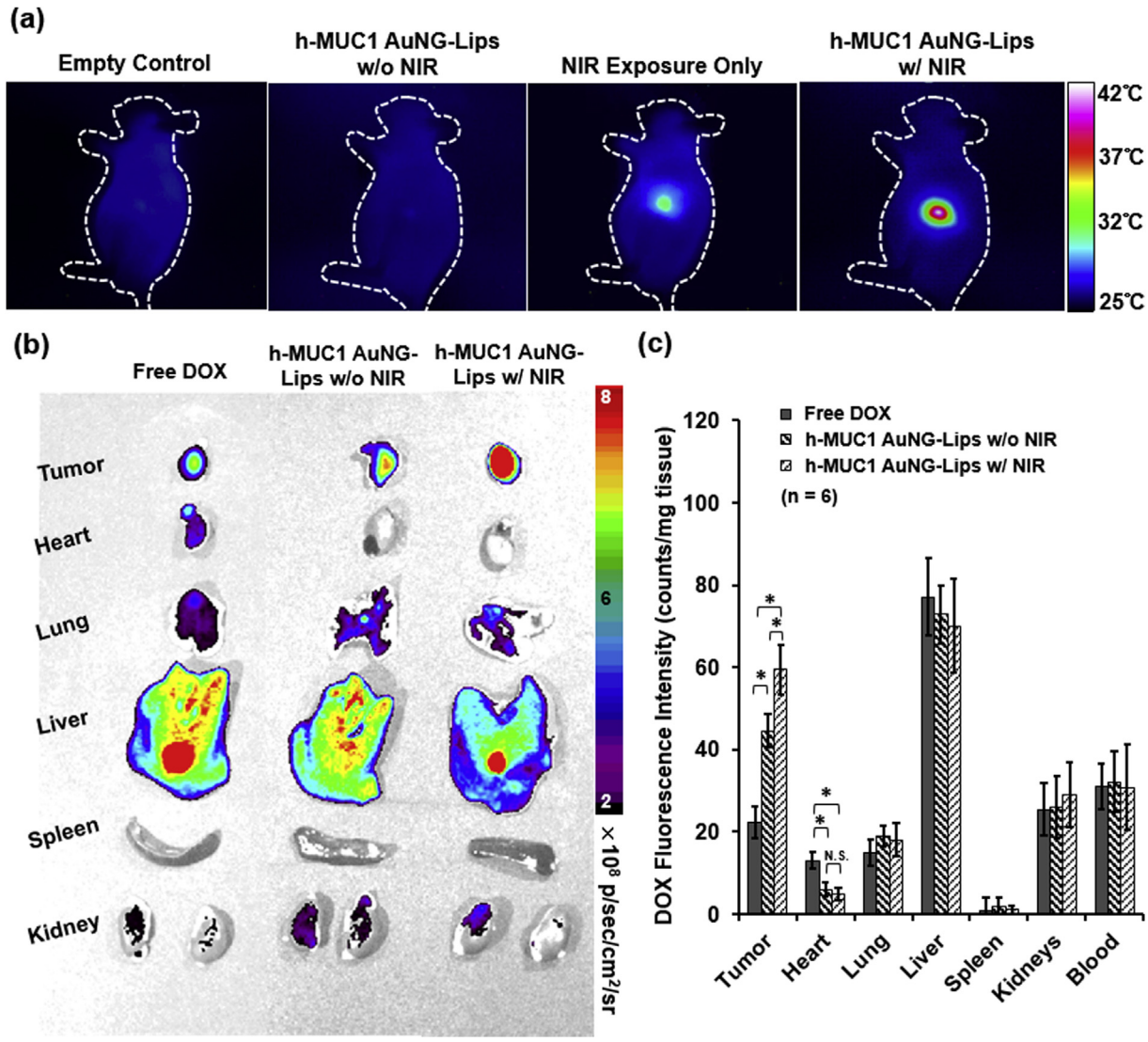

Fig. 7. (a) Thermographic images of MCF-7 tumor-bearing mice that were intravenously injected with h-MUC1 AuNG-Lips one hour after administration following exposure to an NIR laser (~1.2 W/cm^2). (b) Fluorescent images of DOX accumulated in organs and tumors following intravenous injection of mice with free DOX or h-MUC1 AuNG-Lips, with or without NIR treatments, and (c) corresponding fluorescent intensities obtained using a spectrofluorometer (n = 6). N.S.: statistically insignificant; *statistical significance at $P < 0.05$.

received free DOX was minimal, owing to its low tumor accumulation (Fig. 7b and c). Tumor growth was more strongly suppressed by treatment with the h-MUC1 AuNG-Lips ($P < 0.05$), primarily owing to their high tumor targeting ability (Fig. 4a). Notably, the antitumor efficacy for the group that was treated with local heating (w/NIR exposure) was superior to that of the group with no local heating (w/o NIR exposure, $P < 0.05$), revealing the importance of DOX release from the internalized carriers. To maximize therapeutic effectiveness, tumor cells must be subjected to the highest possible concentration of a drug [37].

At the end of the treatment, the antitumor ability of h-MUC1 AuNG-Lips w/NIR was further studied using PET/CT scanners and a radiolabeled tracer ^{18}F-FDG. ^{18}F-FDG is a glucose analog, and has become a standard PET agent of diagnosis of tumors, showing their metabolic activity [38]. The uptake of ^{18}F-FDG is expected to decline greatly as tumor cells die. ^{18}F-FDG PET/CT images in Fig. 8b reveal that the uptake of ^{18}F-FDG by the tumor that received h-MUC1 AuNG-Lips w/NIR (0.78 ± 0.39% ID/g) was lower than that in the saline-treated group (3.17 ± 1.41% ID/g) or in a group that was treated with free DOX (1.54 ± 0.44% ID/g) or h-MUC1 AuNG-Lips alone (w/o NIR, 0.86 ± 0.41% ID/g).

Finally, the tumor sections and heart specimens following treatment were analyzed histologically; the apoptosis of tissue cells in each studied group was also determined using the TUNEL assay. Aggressive tumors are typically characterized by a high nuclear-to-cytoplasmic ratio [39]. A comparison with the saline-treated control revealed that tumor tissues that had received h-MUC1 AuNG-Lips w/NIR exhibited signs of significant cell destruction, including a low nuclear-to-cytoplasmic ratio (H&E stain) and increased cell apoptosis, reflected by many TUNEL-positive cells (Fig. 8c). Notably, the heart that had been treated with free DOX exhibited clear evidence of cytoplasmic vacuolization and myofibrillar loss (H&E stain) together with TUNEL-positive cardiomyocytes. DOX is known to induce DNA damage in cardiomyocytes and is therefore associated with cell apoptosis [40]. The observed cytoplasmic vacuolization/myofibrillar loss and TUNEL-positive cardiomyocyte apoptosis were considerably attenuated in mice that had received h-MUC1 AuNG-liposomes w/NIR. The above empirical findings reveal that the release of DOX from the receptor-mediated internalized h-MUC1 AuNG-Lips can

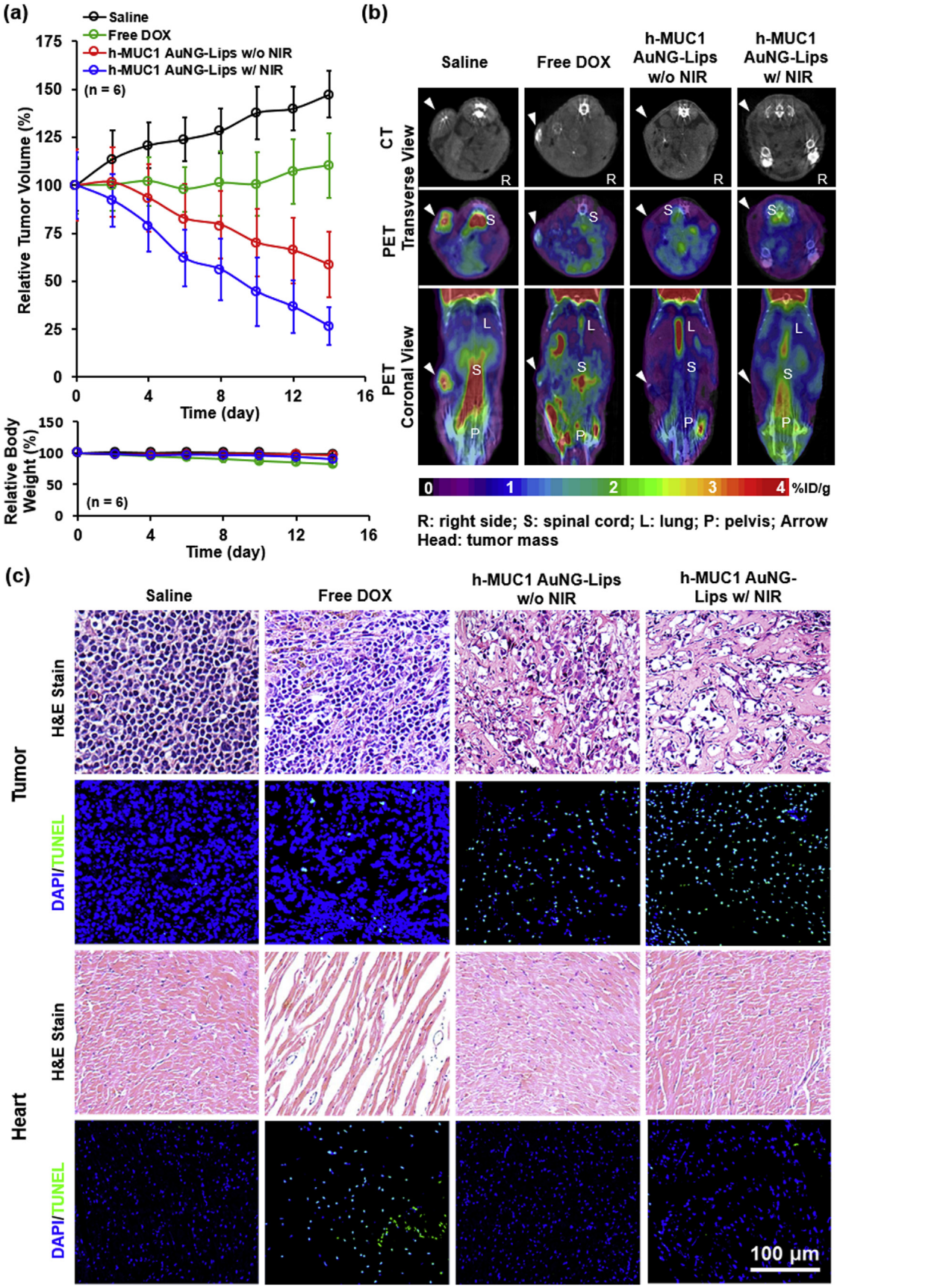

Fig. 8. (a) Changes in relative tumor volume and body weight of mice with MCF-7 tumors in response to various treatments (n = 6), and (b) corresponding ^{18}F-FDG PET/CT images of mice. White arrowhead indicates tumor site. (c) Histological photomicrographs of tumor and heart sections that were stained with H&E, and corresponding TUNEL staining of apoptotic cells in treated groups.

be effectively triggered by localized heating and thereby enhance the tumoricidal destruction of cancer cells while minimizing unwanted side effects, such as cardiotoxicity, providing a promising strategy for treating cancer.

4. Conclusion

In summary, the encapsulation of Au NGs within Lips enables heat to be generated from within those Lips. The h-MUC1 aptamer that is conjugated on the test Lips can act as an activatable molecular beacon, signaling the optimal timing of photothermal heating following systemic administration, to trigger localized drug release within targeted tumor cells. The combined treatment by NIR light irradiation and h-MUC1 AuNG-Lips markedly enhances the killing of cancer cells. These experimental results demonstrate that targeted delivery of both heat and the drug into tumor cells using the developed multifunctional liposomal system is a potential strategy that maximizes therapeutic effectiveness.

Acknowledgements

This work was supported by a grant from the National Science Council (NSC 104-2119-M-007-008), Taiwan (ROC). The PET/CT imaging studies were carried out with the help of the Center of Advanced Molecular Imaging and Translation, Chang Gung Memorial Hospital, Linkou, Taiwan. The authors would also like to thank Prof. Younan Xia of Georgia Institute of Technology for his help with synthesis of gold nanocages.

Appendix A. Supplementary data

Supplementary data related to this article can be found at http://dx.doi.org/10.1016/j.biomaterials.2016.03.040.

References

[1] A. Yavlovich, A. Singh, R. Blumenthal, A. Puri, A novel class of photo-triggerable liposomes containing DPPC: $DC_{8,9}PC$ as vehicles for delivery of doxorubcin to cells, Biochim. Biophys. Acta 1808 (2011) 117–126.
[2] B. Smith, I. Lyakhov, K. Loomis, D. Needle, U. Baxa, A. Yavlovich, J. Capala, et al., Hyperthermia-triggered intracellular delivery of anticancer agent to HER2(+) cells by HER2-specific affibody (ZHER2-GS-Cys)-conjugated thermosensitive liposomes (HER2(+) Affisomes), J. Control. Release 153 (2011) 187–194.
[3] D. Needham, G. Anyarambhatla, G. Kong, M.W. Dewhirst, A new temperature-sensitive liposome for use with mild hyperthermia: characterization and testing in a human tumor xenograft model, Cancer Res. 60 (2000) 1197–1201.
[4] H. Epstein-Barash, G. Orbey, B.E. Polat, R.H. Ewoldt, J. Feshitan, R. Langer, et al., A microcomposite hydrogel for repeated on-demand ultrasound-triggered drug delivery, Biomaterials 31 (2010) 5208–5217.
[5] Y. Wang, M.S. Shim, N.S. Levinson, H.W. Sung, Y. Xia, Stimuli-responsive materials for controlled release of theranostic agents, Adv. Funct. Mater. 24 (2014) 4206–4220.
[6] H. Park, J. Yang, J. Lee, S. Haam, I.H. Choi, K.H. Yoo, Multifunctional nanoparticles for combined doxorubicin and photothermal treatments, ACS Nano 3 (2009) 2919–2926.
[7] L. Cai, Z.Z. Chen, M.Y. Chen, H.W. Tang, D.W. Pang, MUC-1 aptamer-conjugated dye-doped silica nanoparticles for MCF-7 cells detection, Biomaterials 34 (2013) 371–381.
[8] M.F. Chung, K.J. Chen, H.F. Liang, Z.X. Liao, W.T. Chia, Y. Xia, et al., A liposomal system capable of generating CO_2 bubbles to induce transient cavitation, lysosomal rupturing, and cell necrosis, Angew. Chem. Int. Ed. 51 (2012) 10089–10093.
[9] D. Peters, M. Kastantin, V.R. Kotamraju, P.P. Karmali, K. Gujraty, M. Tirrell, et al., Targeting atherosclerosis by using modular, multifunctional micelles, Proc. Natl. Acad. Sci. 106 (2009) 9815–9819.
[10] G.E. Kellogg, J.N. Scarsdale, F.A. Fornari Jr., Identification and hydropathic characterization of structural features affecting sequence specificity for doxorubicin intercalation into DNA double-stranded polynucleotides, Nucleic Acids Res. 26 (1998) 4721–4732.
[11] S.F. Peng, M.T. Tseng, Y.C. Ho, M.C. Wei, Z.X. Liao, H.W. Sung, Mechanisms of cellular uptake and intracellular trafficking with chitosan/DNA/poly(γ-glutamic acid) complexes as a gene delivery vector, Biomaterials 32 (2011) 239–248.
[12] E.F. Pettersen, T.D. Goddard, C.C. Huang, G.S. Couch, D.M. Greenblatt, E.C. Meng, et al., UCSF Chimera–a visualization system for exploratory research and analysis, J. Comput. Chem. 25 (2004) 1605–1612.
[13] J.C. Tseng, H.A. Benink, M.G. McDougall, I. Chico-Calero, A.L. Kung, *In vivo* fluorescent labeling of tumor cells with the HaloTag® technology, Curr. Chem. Genomics 6 (2012) 48–54.
[14] K.J. Chen, E.Y. Chuang, S.P. Wey, K.J. Lin, F. Cheng, C.C. Lin, et al., Hyperthermia-mediated local drug delivery by a bubble-generating liposomal system for tumor-specific chemotherapy, ACS Nano 8 (2014) 5105–5115.
[15] R.W. Ahn, F. Chen, H.M. Chen, S.T. Stern, J.D. Clogston, A.K. Patri, et al., A novel nanoparticulate formulation of arsenic trioxide with enhanced therapeutic efficacy in a murine model of breast cancer, Clin. Cancer Res. 16 (2010) 3607–3617.
[16] C.N. Yeh, K.J. Lin, I.T. Hsiao, T.C. Yen, T.W. Chen, Y.Y. Jan, et al., Animal PET for thioacetamide-induced rat cholangiocarcinoma: a novel and reliable platform, Mol. Imaging Biol. 10 (2008) 209–216.
[17] K.J. Chen, H.F. Liang, H.L. Chen, Y.C. Wang, P.Y. Cheng, H.L. Liu, et al., A thermoresponsive bubble-generating liposomal system for triggering localized extracellular drug delivery, ACS Nano 7 (2013) 438–446.
[18] S.E. Skrabalak, L. Au, X.D. Li, Y. Xia, Facile synthesis of Ag nanocubes and Au nanocages, Nat. Protoc. 2 (2007) 2182–2190.
[19] E. Soussan, S. Cassel, M. Blanzat, I. Rico-Lattes, Drug delivery by soft matter: matrix and vesicular carriers, Angew. Chem. Int. Ed. 48 (2009) 274–288.
[20] C. Boyer, J.A. Zasadzinski, Multiple lipid compartments slow vesicle contents release in lipases and serum, ACS Nano 1 (2007) 176–182.
[21] P.R. Westmark, S.J. Gardiner, B.D. Smith, Selective monosaccharide transport through lipid bilayers using boronic acid carriers, J. Am. Chem. Soc. 118 (1996) 11093–11100.
[22] E.M. Bolotin, R. Cohen, L.K. Bar, N. Emanuel, S. Ninio, Y. Barenholz, et al., Ammonium sulfate gradients for efficient and stable remote loading of amphipathic weak bases into liposomes and ligandoliposomes, J. Liposome Res. 4 (1994) 455–479.
[23] A. Boddien, F. Gärtner, C. Federsel, P. Sponholz, D. Mellmann, R. Jackstell, et al., CO_2-"neutral" hydrogen storage based on bicarbonates and formates, Angew. Chem. Int. Ed. 50 (2011) 6411–6414.
[24] Y. Yang, N. Bajaj, P. Xu, K. Ohn, M.D. Tsifansky, Y. Yeo, Development of highly porous large PLGA microparticles for pulmonary drug delivery, Biomaterials 30 (2009) 1947–1953.
[25] J. Chen, C. Glaus, R. Laforest, Q. Zhang, M. Yang, M. Gidding, et al., Gold nanocages as photothermal transducers for cancer treatment, Small 6 (2010) 811–817.
[26] T.A. Henderson, L.D. Morries, Near-infrared photonic energy penetration: can infrared phototherapy effectively reach the human brain? Neuropsychiatr. Dis. Treat. 11 (2015) 2191–2208.
[27] F.K. Storm, W.H. Harrison, R.S. Elliott, D.L. Morton, Normal tissue and solid tumor effects of hyperthermia in animal-models and clinical-trials, Cancer Res. 39 (1979) 2245–2251.
[28] S. Shin, H.Y. Nam, E.J. Lee, W. Jung, S.S. Hah, Molecular beacon-based quantitation of epithelial tumor marker mucin 1, Bioorg. Med. Chem. Lett. 22 (2012) 6081–6084.
[29] E.D. Matayoshi, G.T. Wang, G.A. Krafft, J. Erickson, Novel fluorogenic substrates for assaying retroviral proteases by resonance energy transfer, Science 247 (1990) 954–958.
[30] P.K. Singh, M.E. Behrens, J.P. Eggers, R.L. Cerny, J.M. Bailey, K. Shanmugam, et al., Phosphorylation of MUC1 by Met modulates interaction with p53 and MMP1 expression, J. Biol. Chem. 283 (2008) 26985–26995.
[31] M.H.G.C. Kranenborg, O.C. Boerman, J.C. Oosterwijk-Wakka, M.C.A. De Weijert, F.H.M. Corstens, E. Oosrterwijk, Two-step radio-immunotargeting of renal-cell carcinoma xenografts in nude mice with anti-renal-cell-carcinoma X anti-DTPA bispecific monoclonal antibodies, Int. J. Cancer 75 (1998) 74–80.
[32] M. Huan, H. Cui, Z. Teng, B. Zhang, J. Wang, X. Liu, et al., *In vivo* anti-tumor activity of a new doxorubicin conjugate via α-linolenic acid, Biosci. Biotechnol. Biochem. 76 (2012) 1577–1579.
[33] P.J. Lou, P.S. Lai, M.J. Shieh, A.J. MacRobert, K. Berg, S.G. Bown, Reversal of doxorubicin resistance in breast cancer cells by photochemical internalization, Int. J. Cancer 119 (2006) 2692–2698.
[34] T.S. Hauck, T.L. Jennings, T. Yatsenko, J.C. Kumaradas, W.C. Chan, Enhancing the toxicity of cancer chemotherapeutics with gold nanorod hyperthermia, Adv. Mater. 20 (2008) 3832–3838.
[35] K. Maruyama, Intracellular targeting delivery of liposomal drugs to solid tumors based on EPR effects, Adv. Drug Deliv. Rev. 63 (2011) 161–169.
[36] T.M. Allen, P.R. Cullis, Liposomal drug delivery systems: from concept to clinical applications, Adv. Drug Deliv. Rev. 65 (2013) 36–48.
[37] J.Y. Lee, S.J. Chung, H.J. Cho, D.D. Kim, Phenylboronic acid-decorated chondroitin sulfate A-based theranostic nanoparticles for enhanced tumor targeting and penetration, Adv. Funct. Mater. 25 (2015) 3705–3717.
[38] A. Almuhaideb, N. Papathanasiou, J. Bomanji, ^{18}F-FDG PET/CT imaging in oncology, Ann. Saudi Med. 31 (2011) 3–13.
[39] F. Burel-Vandenbos, L. Turchi, M. Benchetrit, E. Fontas, Z. Pedeutour, V. Rigau, et al., Cells with intense EGFR staining and a high nuclear to cytoplasmic ratio are specific for infiltrative glioma: a useful marker in neuropathological practice, Neuro Oncol. 15 (2013) 1278–1288.
[40] M. Shi, K. Ho, A. Keating, M.S. Shoichet, Doxorubicin-conjugated immunonanoparticles for intracellular anticancer drug delivery, Adv. Funct. Mater. 19 (2009) 1689–1696.